Geophysical Research Letters

Supporting Information for

Accelerated accumulation of anthropogenic CO_2 drives rapid acidification in the North Pacific subtropical mode water during 1993–2020

Cheng-long Li[1,2,3], Yingxu Wu[1], Xuchen Wang[4], Richard A. Feely[5], Wei-Jun Cai[6], Lei Han[7], Xiaopei Lin[8,9], Di Qi[1,3*]

[1]Polar and Marine Research Institute, Jimei University, Xiamen, China.

[2]Institute of Marine Science and Technology, Shandong University, Qingdao 266237, China.

[3]Third Institute of Oceanography, Ministry of Natural Resources (MNR), Xiamen, China

[4]Key Laboratory of Marine Chemistry Theory and Technology, Ministry of Education, Ocean University of China, Qingdao 266100, China.

[5]Pacific Marine Environmental Laboratory, National Oceanic and Atmospheric Administration, Seattle, WA 98115–6349, USA.

[6]School of Marine Science and Policy, University of Delaware, Newark, DE, USA

[7]China-ASEAN College of Marine Science and Technology, Xiamen University Malaysia, Selangor, Malaysia

[8]Frontier Science Center for Deep Ocean Multispheres and Earth System (FDOMES) and Physical Oceanography Laboratory, Ocean University of China, Qingdao, China

[9]Qingdao National Laboratory for Marine Science and Technology, Qingdao, China

*Corresponding author. Di Qi: qidi@jmu.edu.cn

Contents of this file

Introduction

The supporting information includes 7 text, 3 table, and 10 figures presenting supporting analyses of data from the relevant dataset.

Text S1. Simulation of the North Pacific Subtropical Mode Water

In order to examine the possible mechanism of the subducted C_{ANT}, the characteristics of the North Pacific Subtropical Mode water (STMW) are simulated by a three-dimensional, primitive equation, numerical ocean circulation model MASNUM. This model adopts most of the numerical schemes of the Princeton Ocean Model (POM) but uses a two-time-level algorithm for time stepping. This modification helps remove the computational mode inherent in the three-time-level scheme such as the leapfrog one adopted by POM and many other ocean circulation models (Kantha & Clayson, 2000). It was exemplified that the MASNUM model, besides inheriting the numerical features of POM in other aspects, exhibited better performance in numerical stability. Details of the MASNUM model in both global and regional simulations, comparisons with other mainstream models and its ensuring development can be found in Han (2014) and Zhuang et al. (2016, 2018).

In this case, a global simulation with horizontal resolution of 0.25×0.25 degrees and 31 sigma levels with MASNUM is run under the GEBCO 08 topography (www.gebco.net). The simulation is started from rest with an initial temperature and salinity distribution from WOA09 (Locarnini et al., 2010; Antonov et al., 2010) and forced by surface fluxes of the NCEP-DOE AMIP-II Reanalysis (Kanamitsu et al., 2002). The model is integrated until the total kinetic energy of the global ocean reaches a quasi-equilibrium state (Han, 2014).

An example of how different criterions (θ, σ_θ, potential vorticity) work to define the STMW is demonstrated for a snapshot in August 2018 from the simulation by MASNUM along the 147°E transect in the North Pacific (Figure 1a; Figure S1a in Supporting Information S1; Li et al., 2022a). This water mass appears around 30°N at the depths of 100–400 m, in good agreement with that inferred from Argo data (Cerovečki and Giglio, 2016). From the annual mean perspective, the STMW is well reproduced by the numerical model along the 147°E transect in the North Pacific (Figure S1b).

Taxt S2. Sampling and analytical analyses

The August 2018 cruise was made in the western North Pacific onboard R/V *Tan Kah Kee* from 16 August to 15 September 2018. Depth profiles of temperature and salinity (practical salinity scale of 1978) were determined with a calibrated conductivity-temperature-depth/pressure (CTD) recorder (SBE911 plus, Sea-Bird Scientific, USA). Discrete water samples for dissolved oxygen (DO), dissolved inorganic carbon (DIC), total alkalinity (TA), carbon isotope of DIC ($\Delta^{14}C$ and $\delta^{13}C$), and nutrients (nitrate, nitrite, phosphate and silicate) were collected mainly at depths of 5, 30, 50, 75, 100, 150, 200, 300, 500 and 1000 m using 10-L Niskin bottles mounted with the CTD recorders, whereas samples from up to 2000-m depth were collected at only three stations.

Water samples for DO analyses were collected, fixed, and titrated aboard following the classic Winkler procedure. Any possible nitrite interference in the DO titration was removed by adding 0.01% NaN_3 during subsample fixation (Wong, 2012).

For some DIC samples obtained in August 2018, radiocarbon measurement of DIC (^{14}C) was performed using the Accelerator Mass Spectrometry (AMS) at the Center for Isotope Geochemistry and Geochronology, Qingdao National Laboratory for Marine Science and Technology in Qingdao, China. For ^{14}C analysis, we used a DIC extraction method (Ge et al. 2016) modified from McNichol et al. (1994), with an extraction efficiency >96%. Values of $\Delta^{14}C$ are reported as the modern fraction based on modern reference material, and the precision of $\Delta^{14}C$ analysis was 4‰ or better (Ge et al., 2016). For $\delta^{13}C$ measurements, a water sample (2 mL) was transferred into a 30 ml prevacuumed LABCO vial, acidified and equilibrated, and then automatically analyzed using a Thermo Delta-V Isotope Ratio Mass Spectrometer (IRMS) coupled with a Thermo Gasbench II system. The $\delta^{13}C$ values are reported in ‰ relative to the VPDB standard for DIC with a total uncertainty of ≤0.2‰. After 62 mL (60 mL for $\Delta^{14}C$ and 2 mL for $\delta^{13}C$) seawater was taken from the DIC bottle using syringe, the DIC samples were immediately analysed to avoid the effect of gas exchange.

Water samples for DIC and TA analyses were collected and stored in 250 mL borosilicate glass bottles following the procedure recommended by Dickson et al. (2007), Before sealed with greased (Apiezon-L) ground-glass stoppers, 1 mL of seawater was removed from each sample bottle to allow for thermal expansion, and 100 µL saturated $HgCl_2$ was mixed into the water samples to halt biological activity. They were preserved at room temperature until determination. DIC was measured by an infrared CO_2 detector-based DIC analyzer (AS-C3, Apollo SciTech Inc., United States), and TA was determined at 25°C by the Gran acidimetric

titration using a semi-automated titrator (AS-ALK2, Apollo SciTech Inc., United States). Reproducibility of DIC and TA measurements was at the 0.1% level (Li et al., 2022b). DIC and TA measurements were referred to certified reference materials from Andrew G. Dickson's lab (Scripps Institute of Oceanography, USA) at a precision of ±2 μmol kg^{-1}. Methods for nutrient sampling and measurement are presented in details in Zheng and Zhai (2021).

Text S3. Crossover checks in 1993, 2005 and 2018

Murata et al. (2009) suggested that the NTA value in 1993 had a systematic difference of ~6 μmol kg^{-1} with the value in 2005, e.g., 2311±5 μmol kg^{-1} in 1993 and 2304±2 in 2005 in the layers of 150–300 m depth. In addition, the NTA values are nearly uniform with an average of 2299 ± 7 in upper 300 m in 2018 (Figure S6), in agreement with previously values reported by Millero et al. (1998) (2300±6 μmol kg^{-1}) and Ono et al. (2019) (2297±5 μmol kg^{-1}) in the western North Pacific. Therefore, we perform a systematic adjustment of the NTA in 1993 by subtracting 6 μmol kg^{-1}. This adjustment may induce the C_{ANT} uncertainty of 3 μmol kg^{-1}.

To explore whether systematic adjustments of the AOU, DIC and TA in 1993, 2005 and 2018 are necessary, we made crossover checks in deep water in the KR regime (25°–34°N, 147°–149°E). The result shows that they were generally consistent with each other in the deep waters (Table S1). These comparisons suggest that the measured results of the carbonate system parameters are comparable with each other.

Text S4. Calculations of carbonate-related parameters

Seawater Ω_{arag} and total hydrogen ion scale pH (pH_T; for simplicity, 'pH' in the following text refers to total scale) values were calculated from the concentrations of DIC, TA, temperature, salinity, phosphate, silicate and pressure data using the CO2SYS.xls program (Version 24) (Pelletier et al., 2015). Here Ω_{arag} is defined as the product of calcium and carbonate ion concentrations divided by the stoichiometric solubility product for aragonite (K_{sp}*$_{arag}$), i.e., $\Omega_{arag} = [Ca^{2+}]\times[CO_3^{2-}]/K_{sp}$*$_{arag}$. The dissociation constant of HSO_4^- was taken from Dickson (1990). The carbonic acid dissociation constants of Millero et al. (2006) and the total boron/salinity of Uppström (1974) were used to compute carbonate properties. The K_{sp}*$_{arag}$ values were taken from Mucci (1983), and Ca^{2+} concentrations were assumed to be proportional to salinity (Millero, 1979).

To eliminate the effects of precipitation and evaporation on the seawater carbonate system, the salinity-normalized parameters NTA and NDIC were calculated using the expression NTA = TA/salinity × 35 and NDIC = DIC/salinity × 35, respectively. Apparent oxygen utilization (AOU) was calculated by subtracting the observed DO concentration from the saturated DO concentration (Benson and Krause, 1984), revealing the amount of oxygen consumed since seawater was last under the air–sea equilibrium.

Text S5. Comparison of anthropogenic CO_2 using different methods

The TrOCA method defines a quasi-conservative tracer, TrOCA (Tracer combining O_2, DIC and TA). TrOCA is a reasonable tracer of water masses where changes in TrOCA over time are independent of biology and can be attributed to C_{ANT} penetration. The C_{ANT} can be estimated from the difference between current and pre-industrial TrOCA (TrOCA°) divided by a stoichiometric coefficient. The simplicity of the TrOCA method relies on the fact that a simple formulation for TrOCA° has been proposed based on θ and TA and thus an estimation of C_{ANT} using O_2, DIC, TA and θ. The formulation proposed in Touratier et al. (2007) is used to estimate C_{ANT} as follows:

$$C_{ANT} = [O_2+1.279(DIC-0.5TA)-\exp(7.511-0.01087\theta-7.81\times10^5/TA^2)]/1.279 \quad (1)$$

The overall uncertainty of the approach is 3–6 μmol kg^{-1} due to the random propagation of the uncertainties in the parameters (O_2, DIC, TA and θ) and coefficients (Touratier et al., 2007).

To evaluate the validaty and precision of the TrOCA method in relation to the North Pacific, we compared it with the ΔC* method used for calculating C_{ANT} (Sabine et al., 2002), which is updated from the original ΔC* method developed by Gruber et al. (1996). In brief, the ΔC* method can be expressed as follows:

$$C_{ANT} = \Delta C^* - \Delta C_{diseq}\,, \quad (2)$$

$$\Delta C^* = C_m - C_{280} - \Delta C_{bio}\,, \quad (3)$$

where the quasiconservative tracer (ΔC*) is defined as the difference between the measured DIC (C_m) corrected for biology (ΔC_{bio}) and the air-equilibrated DIC with a preindustrial atmosphere level of CO_2 of 280 μatm at the water surface (C_{280}); ΔC_{diseq} is the air–sea CO_2 disequilibrium expressed in terms of DIC, and the mean value of −6 ± 3 μmol kg^{-1} for the North Pacific taken from Sabine et al. (2002), was used to calculate the C_{ANT}; ΔC_{bio} is the DIC change due to remineralization of organic matter and the dissolution of calcium carbonate particles and denitrification:

$$\Delta C_{bio} = 117/170 \times AOU + 0.5\,(TA - TA^\circ + 16/170 \times AOU) - 106/104 \times (N^* - N^*_{mean}), \quad (4)$$

where 117/170 and 16/170 are the C/O_2 and N/O_2 ratios, respectively (Anderson and Sarmiento, 1994); The denitrification term of $106/104 \times (N^* - N^*_{mean})$, where $N^* = (N - 16P + 2.90)$, was taken from Deutsch et al. (2001), whereas the mean N* (N^*_{mean}) value for our dataset was 0 μmol kg^{-1}; The preformed alkalinity (TA°) is an estimate of the TA that the water had when it

was last at the surface (Gruber et al., 1996). The TA° is necessary to determine the C_{280} and is estimated for the North Pacific using a multiple linear regression of the surface alkalinity values to conservative tracers:

$$TA° = 148.7 + 61.36 \times Salinity + 16/170 \times (O_2 + 170 \times P) - 0.582 \times \theta, \quad (5)$$

where 170 is the O_2/P ratio and θ is potential temperature.

The result showed that the C_{ANT} values using the two methods were consistent with each other at deviation levels of ±6 μmol kg^{-1} below 100 m (Figure S4), within the uncertainty of the TrOCA method (±6 μmol kg^{-1}).

Text S6. Calculation of AOU-corrected pH and Ω_{arag}

To remove the effects from biological processes that might interrupt the decadal trends of pH and Ω_{arag}, we conducted the calculation of AOU-corrected pH and Ω_{arag}. First, we calculated the AOU-corrected DIC ($DIC^{AOU\text{-}corrected}$) as follows:

$$DIC^{AOU\text{-}corrected} = DIC_{obs} - (AOU_{obs} - AOU^{mean}) \times 117/170$$

where DIC_{obs} and AOU_{obs} are the observed DIC and AOU, respectively; AOU^{mean} is the mean AOU value of 24 ± 11 μmol kg^{-1} during 1993-2020, and 117/170 is the C/O_2 ratio (Anderson and Sarmiento, 1994). AOU-corrected pH and Ω_{arag} values were calculated from the $DIC^{AOU\text{-}corrected}$, TA, temperature, salinity, phosphate, silicate and pressure data using the CO2SYS.xls program (Version 24) (Pelletier et al., 2015).

Text S7. Decomposing decadal changes in Ω_{arag} and pH

To evaluate and quantify whether anthropogenic or natural sources were responsible for the progressive OA, we decomposed the decadal changes of STMW Ω_{arag} ($\Delta\Omega_{arag}$) and pH (ΔpH) values during the two periods. Similar to the procedure of Murata & Shu (2012) and Murata et al. (2015), $\Delta\Omega_{arag}$ was firstly decomposed into contributions of individual water chemistry parameter changes of NDIC (ΔNDIC), NTA (ΔNTA), temperature (ΔT) and salinity (ΔS). We further decomposed ΔNDIC into changes in C_{ANT} ($\Delta NDIC^{Anth}$) and organic matter production and remineralization ($\Delta NDIC^{Org}$). Here $\Delta NDIC^{Anth}$ was the difference of C_{ANT} between two surveys based on Eq. (1) in Text S4; $\Delta NDIC^{Org}$ was calculated as $\Delta NDIC^{Org} = \Delta AOU \times 117/170$, where ΔAOU is the difference in AOU between two surveys. Therefore, we used this method to decompose $\Delta\Omega$ as follows,

$$\Delta\Omega_{arag} = (\partial\Omega/\partial NDIC)\Delta NDIC + (\partial\Omega/\partial NTA)\Delta NTA + (\partial\Omega/\partial T)\Delta T + (\partial\Omega/\partial S)\Delta S, \quad (6)$$

$$\Delta\Omega^{\Delta NDIC} = (\partial\Omega/\partial NDIC)\Delta NDIC, \quad (7)$$

$$\Delta\Omega^{\Delta NDIC} = (\Delta NDIC^{Anth}/\Delta NDIC)\Delta\Omega^{\Delta NDIC} + (\Delta NDIC^{Org}/\Delta NDIC)\Delta\Omega^{\Delta NDIC}, \quad (8)$$

$$\Delta\Omega^{Anth} = (\Delta NDIC^{Anth}/\Delta NDIC)\Delta\Omega^{\Delta NDIC}, \quad (9)$$

$$\Delta\Omega^{Org} = (\Delta NDIC^{Org}/\Delta NDIC)\Delta\Omega^{\Delta NDIC}. \quad (10)$$

Therefore,

$$\Delta\Omega_{arag} = \Delta\Omega^{Anth} + \Delta\Omega^{Org} + \Delta\Omega^{\Delta NTA} + \Delta\Omega^{\Delta T} + \Delta\Omega^{\Delta S} + \text{residual}. \quad (11)$$

In Eq. (6), where the $\Delta\Omega_{arag}$, ΔT, ΔS ΔNDIC, and ΔNTA were calculated based on the differences in average water chemistry parameters between two surveys; the four partial derivative terms represent the contributions of changes of average water chemistry parameters on $\Delta\Omega_{arag}$, while keeping the other three parameters constant. In Eq. (7–10), we represent these contributions using the terms: $\Delta\Omega^{\Delta NDIC} = (\partial\Omega/\partial NDIC)\Delta NDIC$, $\Delta\Omega^{Anth} = (\Delta NDIC^{Anth}/\Delta NDIC)\Delta\Omega^{\Delta NDIC}$, $\Delta\Omega^{Org} = (\Delta NDIC^{Org}/\Delta NDIC)\Delta\Omega^{\Delta NDIC}$, $\Delta\Omega^{\Delta NTA} = (\partial\Omega/\partial NTA)\Delta NTA$, $\Delta\Omega^{\Delta T} = (\partial\Omega/\partial T)\Delta T$, and $\Delta\Omega^{\Delta S} = (\partial\Omega/\partial S)\Delta S$. We applied this procedure to the values of each property averaged in the STMW layers of 150 m ($25.1\sigma_\theta$), 200 m ($25.2\sigma_\theta$) and 300 m ($25.4\sigma_\theta$) in the KR region during 1993-2005 and 2005-2018. In a similar manner to the decomposition of $\Delta\Omega_{arag}$, we also decomposed ΔpH. Note that, the effects of precipitation and dissolution of $CaCO_3$ on Ω_{arag} and pH were generally considered minor in the upper ~400

213 m of the western subtropical gyre (Murata & Shu, 2012; Murata et al., 2015) and were
214 attributed to the residual.
215
216

Table S1. Crossover checks in deep water (~1000 m) in the Kuroshio Recirculation regime (25–32°N, 147–149°E). TA values in 1993 have been adjusted according to Text S3.

Time	AOU (μmol kg^{-1})	DIC (μmol kg^{-1})	TA (μmol kg^{-1})	NTA (μmol kg^{-1})	$\Delta^{14}C$ (‰)	$\delta^{13}C$ (‰)
Aug 2018	269 ± 7	2332 ± 13	2346 ± 11	2398 ± 8	−169 ± 37	−0.38 ± 0.04
May 2005	266 ± 9	2327 ± 13	2344 ± 10	2396 ± 7	−171 ± 24	−0.44 ± 0.04
Ocotber 1993	266 ± 14	2327 ± 16	2344 ± 11	2395 ± 8	−167 ± 27	−0.41 ± 0.06

Table S2. Rates of the decadal trends in C_{ANT}, pH and Ω_{arag} when using 3 cruises (1993, 2005 and 2018) or 124 cruises (26-year GLODAP and JMA datasets during 1993-2020) regularly conducted in the North Pacific subtropical mode water.

Periods	Dataset	Rate of C_{ANT} increase (μmol kg^{-1} yr^{-1})	Rate of Ω_{arag} decrease (yr^{-1})	Rate of pH decrease (yr^{-1})
1993-2005	1993 and 2005	0.76 ± 0.07	-0.0078 ± 0.0024	-0.0011 ± 0.0002
1993-2005	GLODAP	0.68 ± 0.31	-0.0074 ± 0.0067	-0.0015 ± 0.0008
2005-2018	2005 and 2018	1.76 ± 0.06	-0.0242 ± 0.002	-0.0050 ± 0.0003
2005-2020	GLODAP and JMA	1.51 ± 0.06	-0.0176 ± 0.0029	-0.0028 ± 0.0005

Table S3. Rates of the NDIC, C_{ANT}, Ω_{arag} and pH changes for different periods in KR surface waters and STMW. Note that the rates of NDIC, Ω_{arag} and pH in KR surface waters are from Ono et al. (2019), and the rate of NDIC change is entirely attributed to the C_{ANT} change. The rates in the STMW refer to Figure 4 and Figure S7. p <0.05 indicates statistical significance at the 95% confidence level.

Periods	Water	Rate of NDIC increase (μmol kg^{-1} yr^{-1})	Rate of C_{ANT} increase (μmol kg^{-1} yr^{-1})	Rate of Ω_{arag} decrease (yr^{-1})	Rate of pH decrease (yr^{-1})
1993-2005	Surface	0.8 ($p < 0.05$)	/	-0.008 ($p < 0.05$)	-0.0014 ($p < 0.05$)
1993-2005	STMW	0.8 ($p = 0.19$)	0.7 ($p < 0.05$)	-0.0074 ($p = 0.29$)	-0.0015 ($p = 0.12$)
2005-2017	Surface	1.6 ($p < 0.05$)	/	-0.018 ($p < 0.05$)	-0.0028 ($p < 0.05$)
2005-2017/2020	STMW	1.8 ($p < 0.01$)	1.5 ($p < 0.05$)	-0.0176 ($p < 0.01$)	-0.0028 ($p < 0.01$)

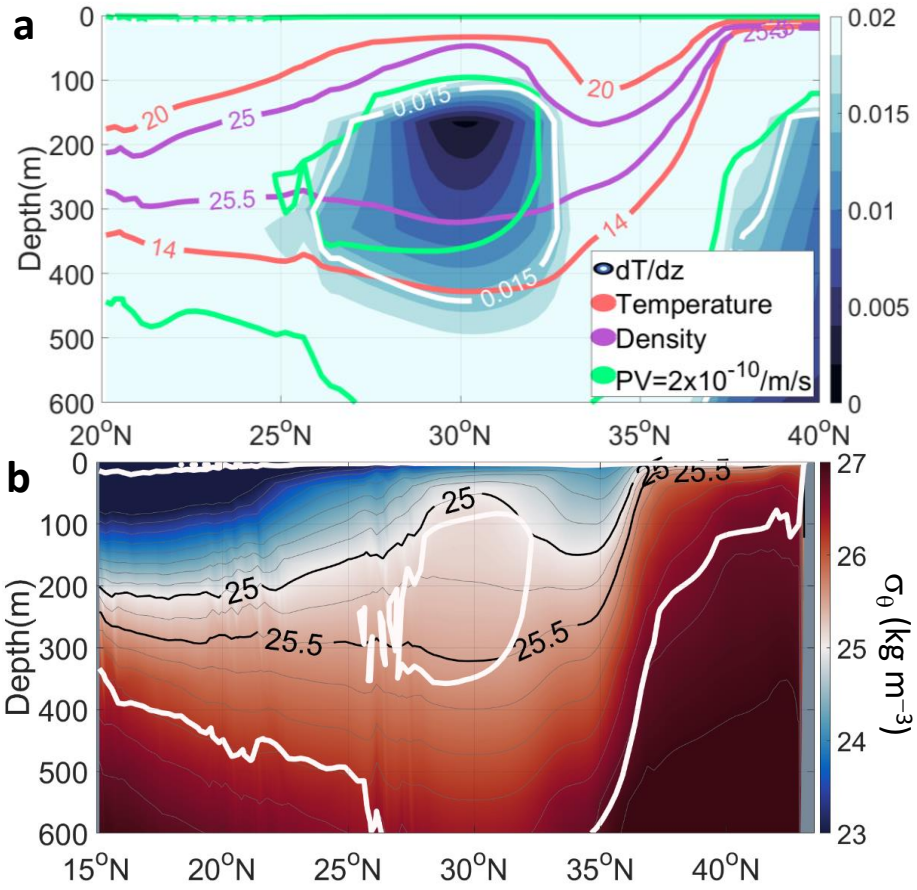

Figure S1. (a) Different criterions to define the STMW along the 147°E transect in the North Pacific. Color fills denote the vertical derivative of the potential temperature, dT/dz. Pink, purple and green lines represent contour lines of potential temperature, density and PV, respectively. White lines denote the dT/dz criterion adopted in Tsubouchi et al. (2016). The data is produced by a global run of the MASNUM model detailed in text. (b) Latitudinal variations of the annual mean potential density (σ_θ) and the PV contours of 2×10^{-10} m^{-1} s^{-1} (white contours) along the 147°E transect in the North Pacific produced by the MASNUM model.

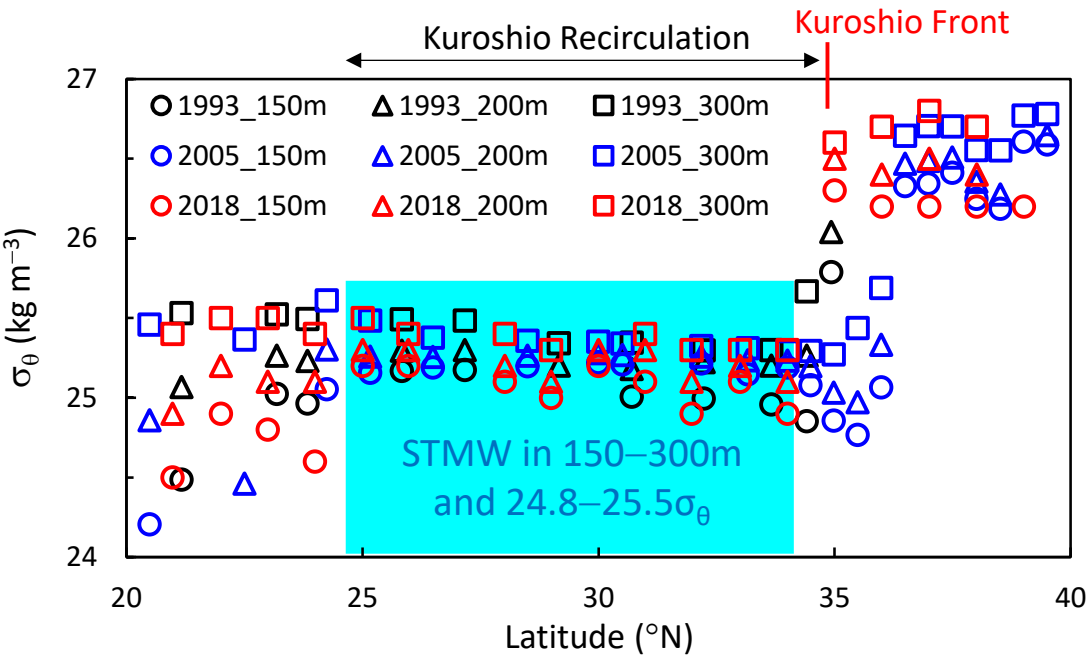

Figure S2. Latitudinal distributions of the potential density (σ_θ) in the STMW layers of 150m, 200m and 300m (24.8–25.5σ_θ) along the 147°–149°E sections.

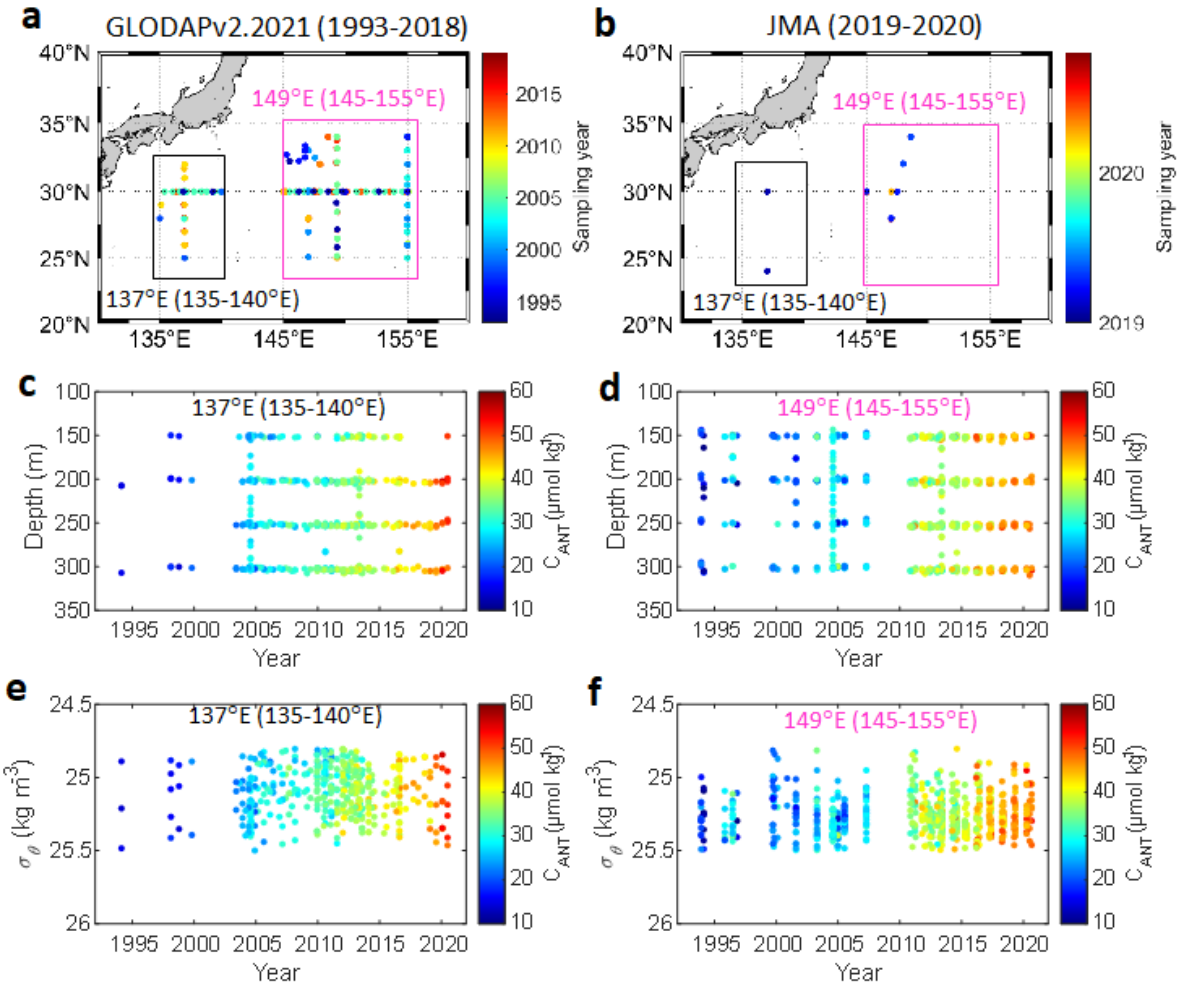

Figure S3. (a–b) All stations of C_{ANT} data in the two STMW distribution regions mainly along 149°E (145°E–155°E, 25°N–34°N) and 137°E (135°E–140°E, 24°N–32°N) during 1993–2018 from GLODAPv2.2021 and during 2019–2020 from the Japan Meteorological Agency (JMA) website (https://www.data.jma.go.jp). (c–d) Depths of STMW C_{ANT} data in 150–300m in the two regions. (e–f) Potential density (σ_θ) of STMW C_{ANT} data within 150–300m and 24.8–25.5σ_θ in the two regions.

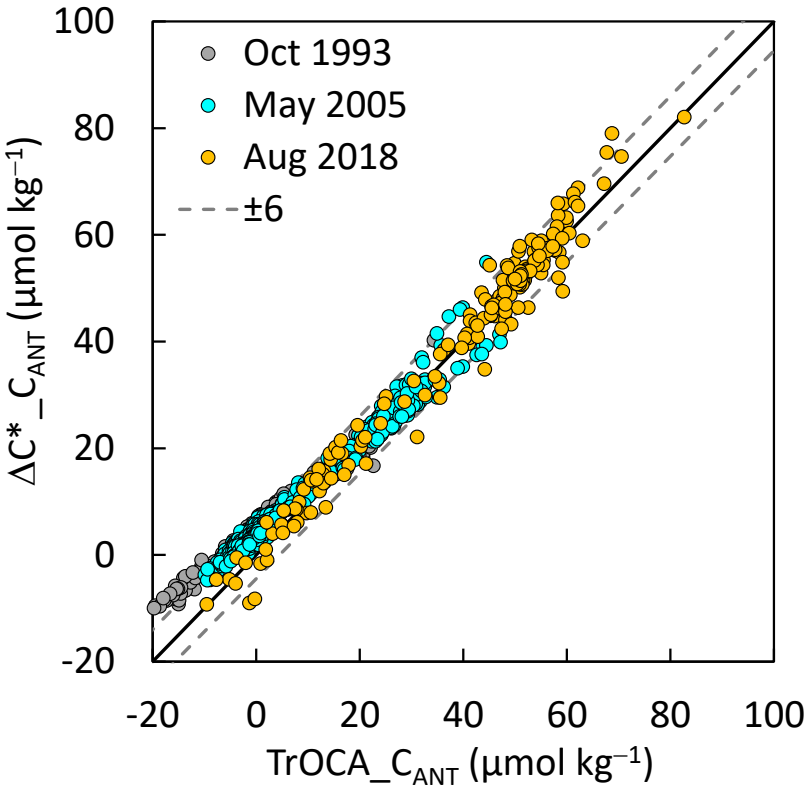

Figure S4. Comparison of C_{ANT} values calculated from TrOCA method (TrOCA_C_{ANT}) and ΔC* method (ΔC*_C_{ANT}) below 100 m in August 2018, May 2005 and October 1993 along 147°–149°E (20°–40°N) in the western North Pacific.

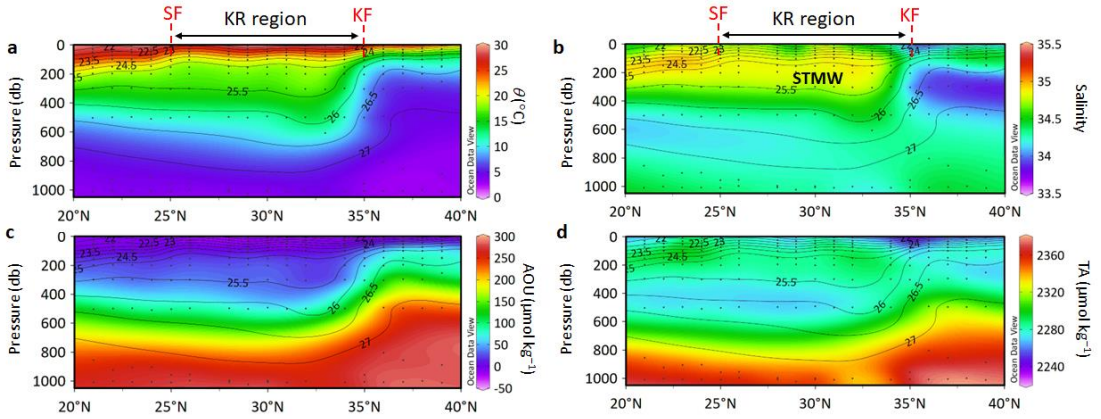

Figure. S5. Latitudinal variations in potential temperature (θ), salinity, AOU and TA along the 147°E transect in August 2018, drawn with Ocean Data View software (Schlitzer, R., 2015, Ocean Data View 4, http://odv.awi.de). Black contours represent the potential density. KF = Kuroshio front, SF = subtropical front, KR = Kuroshio Recirculation, STMW = subtropical mode water.

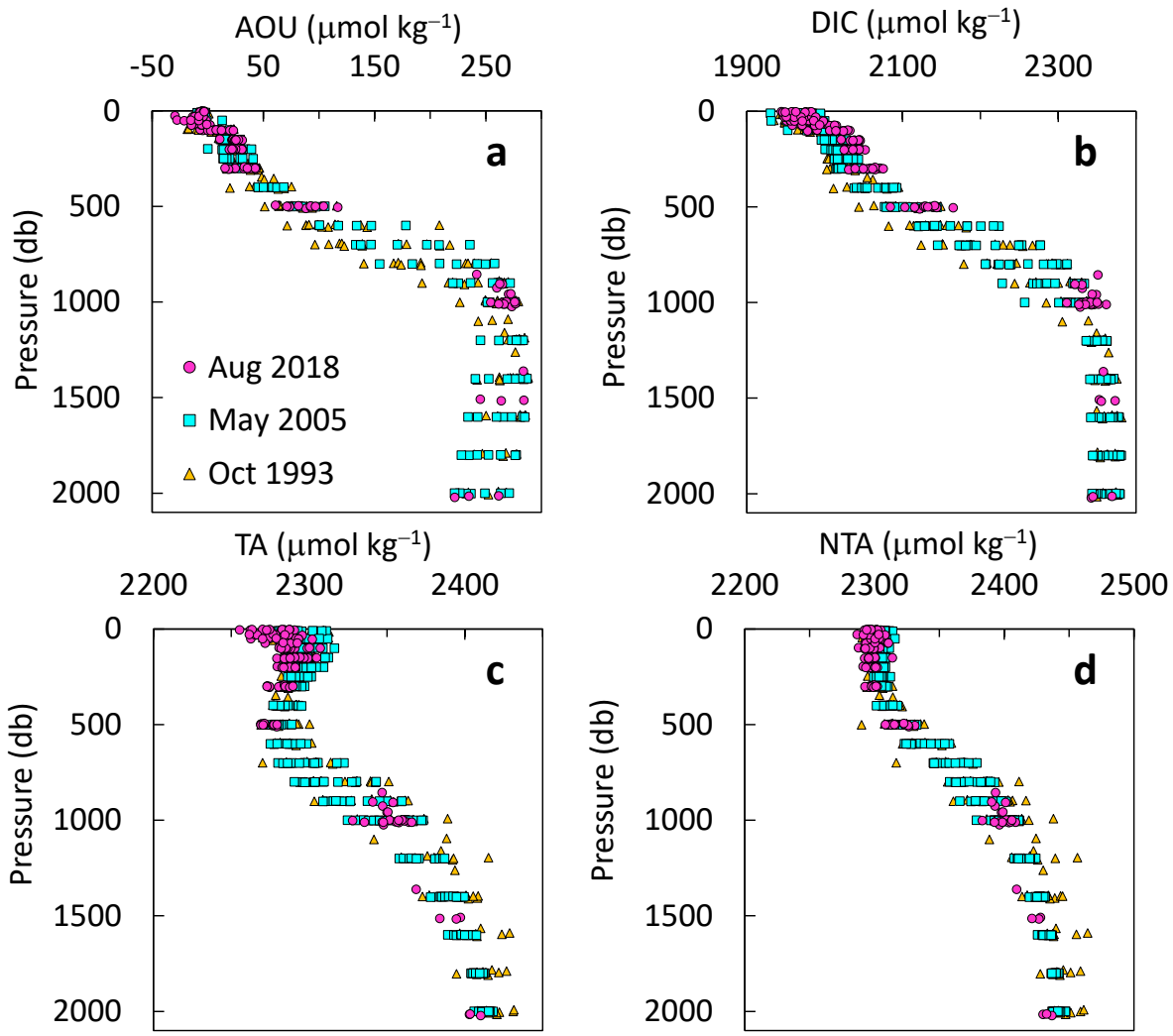

Figure S6. (a–d) Vertical profiles of water AOU, DIC, TA and salinity-normalized TA (NTA) in August 2018 (red circles), May 2005 (Cyan rectangles) and October 1993 (yellow triangles) in upper 2000 m depth south of the Kuroshio Extention (147°–149°E, 20°N–34°N).

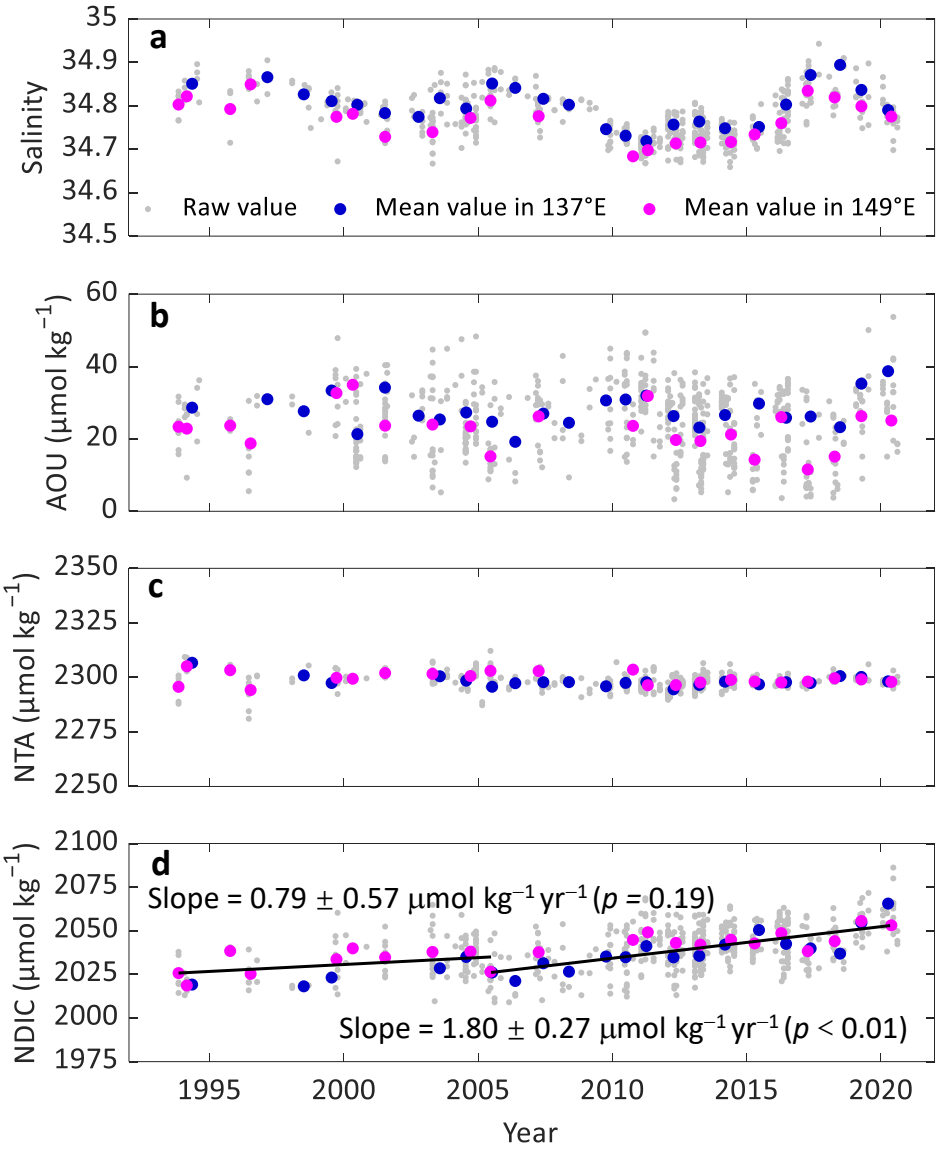

Figure S7. Temporal changes in salinity, AOU, and salinity-normalized TA (NTA) and DIC (NDIC) in the STMW (200–250 m and 24.8–25.5σ_θ) during 1993–2020 around the 149°E section (25°–34°N, 145°–155°E) and 137°E section (24°–32°N, 135°–140°E). The grey dots represent the raw data, and the blue and red dots indicate the annual means. The black lines represent linear regression to all annual mean data during 1993–2005 and 2005–2020; slopes (mean ± standard errors) indicate rates of change; p <0.05 indicates statistical significance at the 95% confidence level.

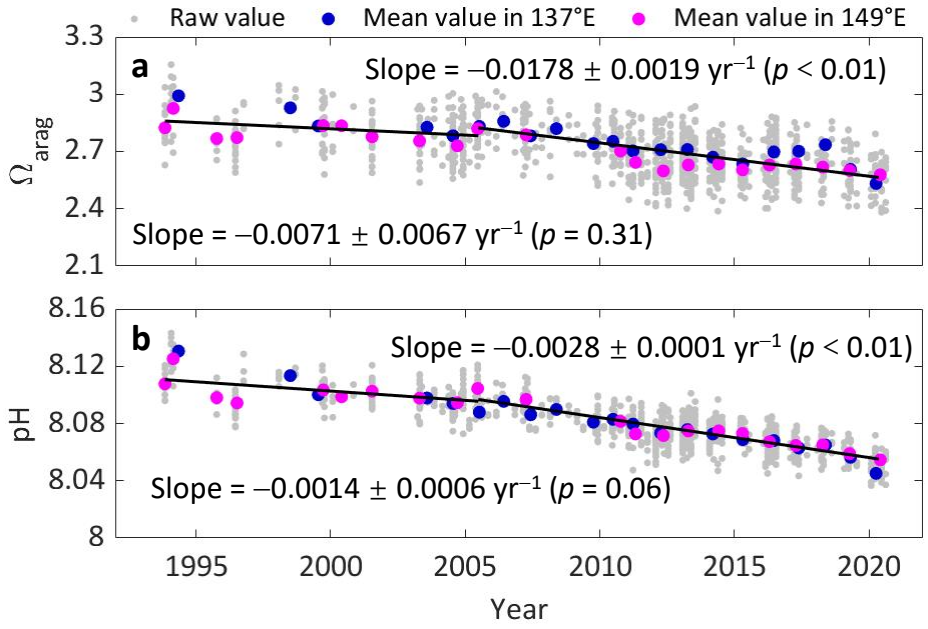

Figure S8. Same as Figure S7 but for the AOU-corrected (to the mean AOU value of 24±11 μmol kg^{-1} during 1993–2020) Ω_{arag} and pH based on Text S7.

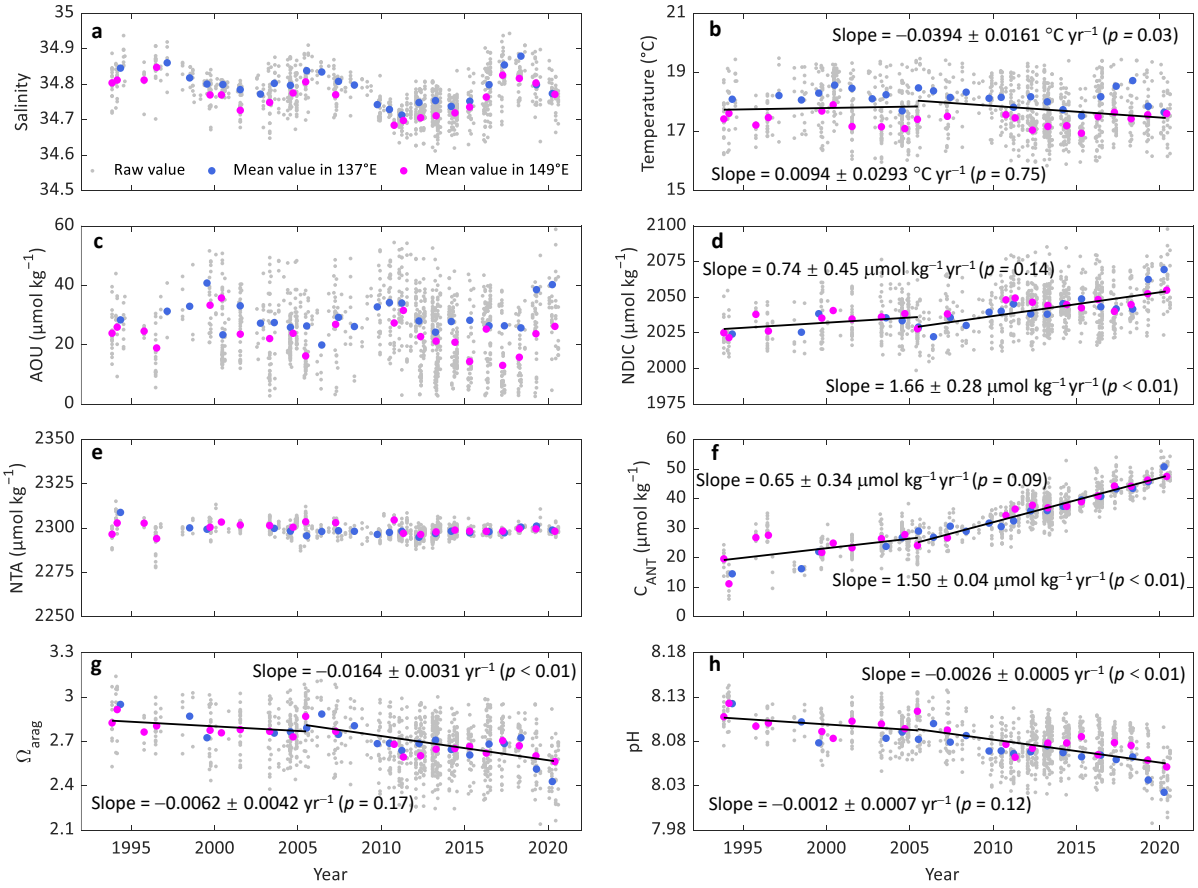

Figure S9. Same as Figure S7 but for the STMW within 150–300 m and 24.8–25.5σ_θ.

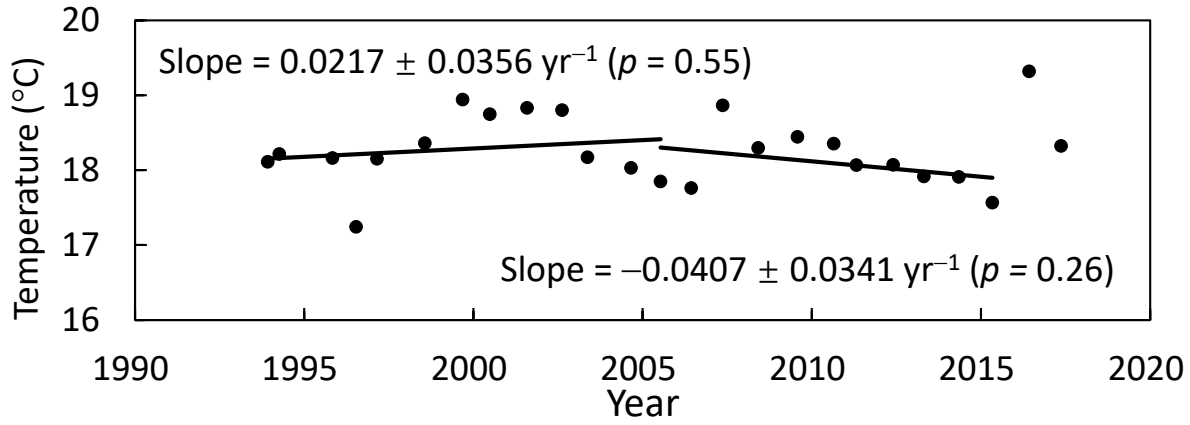

Figure S10. Wintertime (February) sea surface temperature in the main STMW formation region south of Kuroshio Extention (Kuroshio Recirculation region: 30°–34°N, 145°–160°E) during 1993–2017. The NOAA Extended Reconstructed Sea Surface Temperature (ERSST) v4 is obtained from the website (http://www.ncdc.noaa.gov).

References

Anderson, L. A., & Sarmiento, J. L. (1994). Redfield ratios of remineralization determined by nutrient data analysis. *Global Biogeochemical Cycles, 8*, 65–80. https://doi.org/10.1029/93GB03318

Antonov, J. I., Seidov, D., Boyer, T. P., Locarnini, R. A., Mishonov, A. V., Garcia, H. E., et al. (2010). World Ocean Atlas 2009, Volume 2: Salinity. In: S. Levitus, Ed. NOAA Atlas NESDIS 69, U.S. Government Printing Office, Washington DC, USA. 184 pp. https://www.nodc.noaa.gov/OC5/indprod.html

Benson, B. B., & Krause, D. (1984). The concentration and isotopic fractionation of oxygen dissolved in fresh water and seawater in equilibrium with the atmosphere. *Limnology and Oceanography, 29*, 620–632. https://doi.org/10.4319/lo.1984.29.3.0620

Cerovečki, I., & Giglio, D. (2016). North Pacific subtropical mode water volume decrease in 2006–2009 estimated from Argo observations: influence of surface formation and basin scale oceanic variability. *Journal of Climate, 29*, 2177–2199. https://doi.org/10.1175/JCLI-D-15-0179.1

Deutsch, C., Gruber, N., Key, R. M., Sarmiento, J. L., Ganachaud, A. (2001). Denitrification and N_2 fixation in the Pacific Ocean. *Global Biogeochemical Cycles, 15*, 483–506. https://doi.org/10.1029/2000GB001291

Dickson, A. G., Sabine, C. L., & Christian, J. R. (2007). *Guide to best practices for ocean CO_2 measurements, PICES Special Publication* (Vol. 3(8), p. 191). Sidney, British Columbia, Canada: North Pacific Marine Science Organization.

Dickson, A. G. (1990). Standard potential of the reaction: $AgCl(s)+1/2H_2(g)=Ag(s)+HCl(aq)$, and the standard acidity constant of the ion HSO_4^- in synthetic sea water from 273.15 to 318.15 K. *The Journal of Chemical Thermodynamics, 22*(2), 113–127. https://doi.org/10.1016/0021-9614(90)90074-Z

Ge, T. T., Wang, X. C., Zhang, J., Xue, Y. J., & Luo, C. L. (2016). Dissolved inorganic radiocarbon in the northwest Pacific continental margin. *Radiocarbon*, *58*(3), 517–529 https://doi.org/10.1017/RDC.2016.23

Gruber, N., Sarmiento, J. L., & Stocker, T. F. (1996). An improved method for detecting anthropogenic CO_2 in the oceans. *Global Biogeochemical Cycles, 10*, 809–837. https://doi.org/10.1029/96GB01608

Han, L. (2014). A two-time-level split-explicit ocean circulation model (MASNUM) and its validation. *Acta Oceanologica Sinica, 33*(11), 11–35. https://doi.org/10.1007/s13131-014-0553-z

Kanamitsu, M., Ebisuzaki, W., Woollen, J., Yang, S.-K., Hnilo, J. J., Fiorino, M., & Potter, G. L. (2002). NCEP–DOE AMIP-II Reanalysis (R-2). *Bulletin of the American Meteorological Society, 83*(11), 1631−1643. https://doi.org/10.1175/BAMS-83-11-1631

Kantha, L. H., & Clayson, C. A. (2000). Numerical Models of Oceans and Oceanic Processes. International Geophysics Series, 66, Academic Press, San Diego, USA. 750 pp. https://www.sciencedirect.com/bookseries/international-geophysics/vol/66/suppl/C

Li, C.-L., Han, L., Zhai, W.-D., Qi, D., Wang, X.-C., Lin, H.-M., et al. (2022a). Storage and redistribution of anthropogenic CO_2 in the western North Pacific: The role of subtropical mode water transportation. *Fundamental Research*, in press. https://doi.org/10.1016/j.fmre.2022.05.001

Li, C.-L., Zhai, W.-D., & Qi, D. (2022b). Unveiling controls of the latitudinal gradient of surface pCO_2 in the Kuroshio Extension and its recirculation regions (northwestern North Pacific) in late spring. *Acta Oceanologica Sinica, 41*(5), 108–121, http://www.aosocean.com/article/doi/10.1007/s13131-021-1949-1

Locarnini, R. A., Mishonov, A. V., Antonov, J. I., Boyer, T. P., Garcia, H. E., Baranova, O. K., et al. (2010). World Ocean Atlas 2009, Volume 1: Temperature. In: S. Levitus, Ed. NOAA Atlas NESDIS 68, U.S. Government Printing Office, Washington DC, USA. 184 pp. https://www.nodc.noaa.gov/OC5/indprod.html

McNichol, A. P., Jones, G. A., Hutton, D. L., & Gagnon, A. R. (1994). The rapid preparation of seawater $\sum CO_2$ for radiocarbon analysis at the National Ocean Sciences AMS facility. *Radiocarbon*, *36*(2), 237–246. https://doi.org/10.1017/S0033822200040522

Millero, F. J. (1979). The thermodynamics of the carbonate system in seawater. *Geochimica et Cosmochimica Acta*, *43*(10), 1651–1661. https://doi.org/10.1016/0016-7037(79)90184-4

Millero, F. J., Lee, K., & Roche, M. (1998). Distribution of alkalinity in the surface waters of the major oceans. *Marine Chemistry, 60*, 111–130. https://doi.org/10.1016/S0304-4203(97)00084-4

Millero, F. J., Graham, T. B., Huang, F., Bustos-Serrano, H., & Pierrot, D. (2006). Dissociation constants of carbonic acid in seawater as a function of salinity and temperature. *Marine Chemistry, 100*, 80–94. https://doi.org/10.1016/j.marchem.2005.12.001

Mucci, A. (1983). The solubility of calcite and aragonite in seawater at various salinities, temperatures, and one atmosphere total pressure. *American Journal of Science, 283*(7), 780–799. https://doi.org/10.2475/ajs.283.7.780

Murata, A., Kumamoto, Y., Sasaki, K., Watanabe, S., & Fukasawa, M. (2009). Decadal increases of anthropogenic CO_2 along 149°E in the western North Pacific. *Journal of Geophysical Research*, *114*, C04018. https://doi.org/10.1029/2008JC004920

Murata, A., & Saito, S. (2012). Decadal changes in the $CaCO_3$ saturation state along 179°E in the Pacific Ocean. *Geophysical Research Letters*, *39*(12), L12604. https://doi.org/10.1029/2012GL052297

Murata, A., Hayashi, K., Kumamoto, Y., & Sasaki K. (2015). Detecting the progression of ocean acidification from the saturation state of $CaCO_3$ in the subtropical South Pacific. *Global Biogeochemical Cycles*, *29*(4), 463–475. https://doi.org/10.1002/2014GB004908

Ono, H., Kosugi, N., Toyama, K., Tsujino, H., Kojima, A., Enyo, K., et al. (2019). Acceleration of ocean acidification in the Western North Pacific. *Geophysical Research Letters*, *46*(22), 13161−13169. https://doi.org/10.1029/2019GL085121

Pelletier, G. J., Lewis, E., & Wallace, D. W. R. (2015). CO2SYS.XLS: A calculator for the CO_2 system in seawater for Microsoft Excel/VBA, Version 24, Washington State Department of Ecology, Olympia, Washington.

Sabine, C. L., Feely, R. A., Key, R. M., Bullister, J. L., Millero, F. J., Lee, K., et al. (2002). Distribution of anthropogenic CO_2 in the Pacific Ocean. *Global Biogeochemical Cycles, 16*, 1083. https://doi.org/10.1029/2001GB001639

Touratier, F., Azouzi, L., & Goyet, C. (2007). CFC-11, $\Delta^{14}C$ and ^{3}H tracers as a means to assess anthropogenic CO_2 concentrations in the ocean. *Tellus B, 59*, 318–325. https://doi.org/10.1111/j.1600-0889.2006.00247.x

Uppström, L. R. (1974). The boron/chlorinity ratio of deep-sea water from the Pacific Ocean. *Deep Sea Research and Oceanographic Abstracts*, *21*, 161–162. https://doi.org/10.1016/0011-7471(74)90074-6

Wong, G. T. F. (2012). Removal of nitrite interference in the Winkler determination of dissolved oxygen in seawater. *Marine Chemistry, 130*, 28–32. https://doi.org/10.1016/j.marchem.2011.11.003

Zheng, L.-W., & Zhai, W.-D. (2021). Excess nitrogen in the Bohai and Yellow seas, China: distribution, trends, and source apportionment. *Science of The Total Environment, 794*, 148702. https://doi.org/10.1016/j.scitotenv.2021.148702

Zhuang, Z. P., Yuan, Y. L., Zhang, J., Han, L., & Yang, J. G. (2016). An efficient parallel algorithm for ocean circulation numerical model based on irregular rectangle decomposition scheme. *Acta Oceanologica Sinica, 35*(4), 18–23. https://doi.org/10.1007/s13131-016-0855-4

Zhuang, Z. P., Yuan, Y. L., & Yang, G. B. (2018). An ocean circulation model in σS-z-σB hybrid coordinate and its validation. *Ocean Dynamics, 68*, 159–175. https://doi.org/10.1007/s10236-017-1124-6